derivative [27] of the two-point tensor a with respect to the time-dependent tensor function $\frac{1}{J}F$ with $J = detF$ and F being measured from an arbitrarily fixed reference configuration:

$$tr(L)a + \frac{da}{dt} - aL^T = \frac{d\left(aJF^{-T}\right)}{dt}\frac{1}{J}F^T = 0. \tag{27}$$

With the material velocity considered as a given field, this is simply the linearization of the statement that the convected derivative of the two-point tensor field α vanishes, i.e.

$$div(v)\alpha + \frac{d\alpha}{dt} - \alpha L^T = 0. \tag{28}$$

This is the Lagrangian equivalent of (18) under the assumption that $V = 0$, $s = 0$ and $div\ \alpha = 0$ [17], stating that the Burgers vector content of a material area patch remains constant in the absence of dislocation sources and if the existing dislocations threading the patch do not move with respect to the material.

We note that with the velocity gradient field considered as a given input, (26) constitutes a pointwise system of ordinary differential equations (ODE) for the perturbation array a. For approximate analysis of stability of this system, we consider it as a constant coefficient system of ODE governed by the velocity gradient field at every point. For the analysis of growth of perturbations it helps to consider the components of a_{ij} as a 9×1 vector A and $(v_{j,m}\delta_{ir} - v_{k,k}\delta_{ir}\delta_{jm})$ as a 9×9 array denoted by $\mathscr{N}$ to write (26) as

$$\frac{dA}{dt} = \mathscr{N}A. \tag{29}$$

If at any stage of deformation an eigenvalue of $\mathscr{N}$ has a positive real part at any point of the body, then that state is deemed to be 'linearly unstable' and susceptible to the nucleation of a dislocation. Of course, linear stability is only conclusive with respect to stability, so for conditions of instability, we treat such positivity as a necessary condition and probe magnitudes of the real parts of the eigenvalues as well.

We denote the maximum of the real parts of the eigenvalues of $\mathscr{N}$ at any point by the value of the field η at that point.

To understand growth of the dislocation density field at the instant of incipient instability, we note that (26) implies

$$\frac{d\left(a_{ij}a_{ij}\right)}{dt} = 2a_{ij}(D_{jm}\delta_{ir} - D_{kk}\delta_{ir}\delta_{jm})a_{rm}, \tag{30}$$

where D is the symmetric part of the velocity gradient L, and we observe that our nucleation criterion has the correct limiting behavior in the case of rigid motions, implying that no growth of perturbations in dislocation density (i.e. nucleation) is possible from a dislocation-free state in the case of arbitrary rigid motions. More interestingly, we note the following facts.

B. Convected rate vs. Jaumann rate

While in our theory the convected derivative with respect to $\left(\frac{1}{J}F\right)$ appearing in (28) is a non-negotiable ingredient implied by the necessity of doing calculus on a body occupying coherent regions of space parametrized by time, considerations of frame-indifference alone would allow the convected rate to be posed as any appropriate objective rate for the two-point tensor field α. In particular, if one were to arbitrarily choose the analog of the Jaumann rate for this two-point tensor field, i.e. the convected rate with respect to the orthogonal tensor R^* that at each point of the body satisfies $\frac{dR^*}{dt} = \Omega^* R^*$, where Ω^* is the material spin (the skew-symmetric part of the velocity gradient L), then (26), (28), and (30) imply that nucleation would never be possible.

C. Volterra and Somigliana distributions

Further insight into the possible predictions of nucleation from (26) can be obtained by considering velocity fields with 'planar' spatial variation in only the x_1 and x_2 directions and dislocation density perturbations to be constrained to only $a_{i3} \neq 0$ (i.e. straight dislocations with x_3 as line direction). Then (25) directly implies

$$\frac{da_{i3}}{dt} = -v_{r,r} a_{i3}. \tag{31}$$

In particular, planar simple shearing in the x_1 direction (only the v_1 component as non-zero) on planes normal to x_2 with variation only in the x_2 direction can cause no nucleation of straight dislocations threading the $x_1 - x_2$ plane (assuming these are the only type of dislocations that are allowed). However, if there exists a slip-direction gradient of the shear strain-rate field, i.e. $v_{1,21}$ is non-zero, then the compatibility of the velocity gradient field (equality of the second partial derivatives) implies that $v_{1,1}$ must be non-zero at such points and that this can cause nucleation of straight edge dislocations according to our criterion (and similarly for the nucleation of straight screws corresponding to shearing in the x_3 direction with in-plane spatial variations). In particular, if we have an incipient slip embryo where the v_1 component is uniform in the x_1 direction except for sharp drop-offs at the boundary of the embryo, then the possibility of a nucleating a Volterra edge dipole exists as shown in Fig. 7b and 7d. On the other hand, if the v_1 field varies smoothly along the x_1 direction within the embryo then the possibility nucleating a true continuously distributed dislocation density field exists, corresponding to a Somigliana distribution, as shown in Fig. 7a and 7c. In the simulations of sec. IV, a Somigliana distribution is what appears to nucleate in atomic configurations under load.

Equation (31) was based on the assumption that only $a_{i3} \neq 0$; however, we note here that Figs. 7c and 7d are plots of the η field from calculations that allows for all possible dislocation density perturbations, using the driving velocity fields shown in Figs. 7a and 7b, respectively. In sec. V, results utilizing actual atomistic, nanoindentation velocity fields are reported.

D. Shear band/phase boundary and dislocation nucleation

The nucleation of a phase boundary or a shear band without terminations within the body are cases that are controlled by the occurrence of localized transverse gradients of the velocity

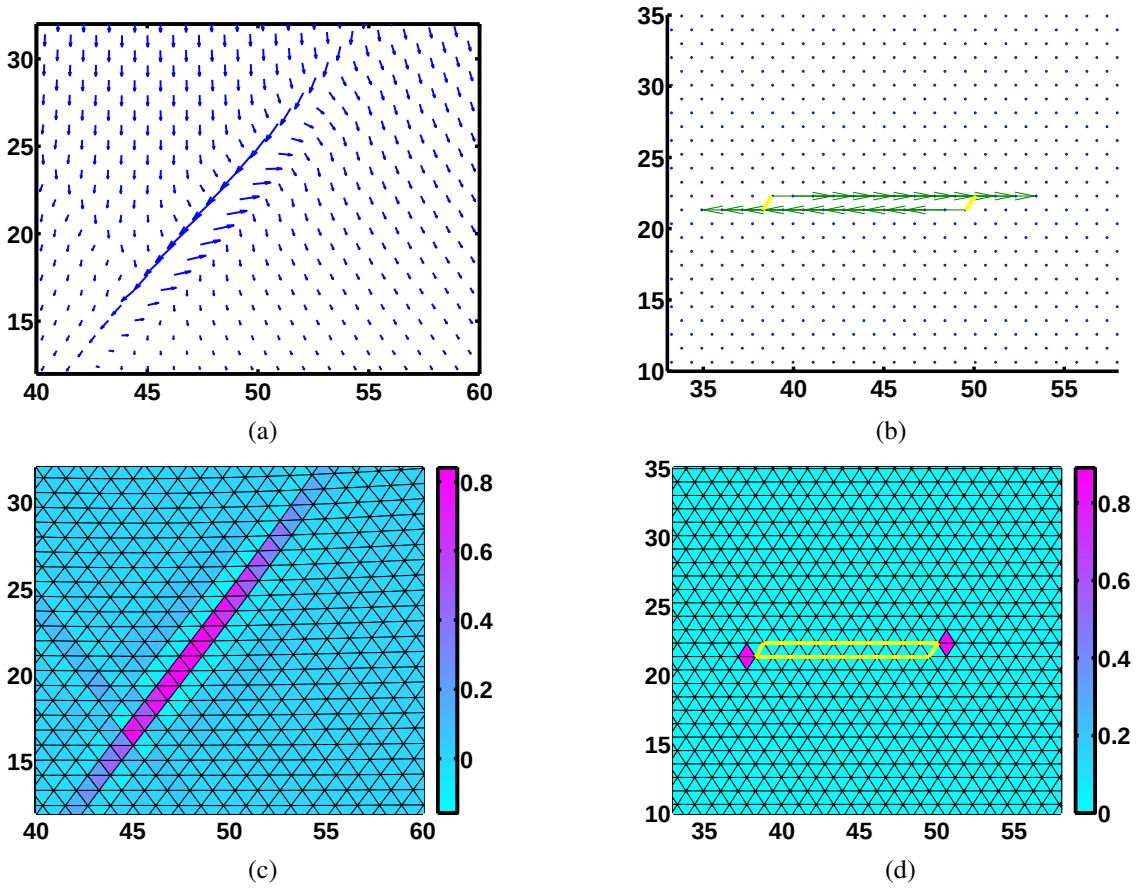

Fig. 7: L-J crystal, O_1 (a) Velocity field for R = 120, just before nucleation. (b) Idealized velocity field for nucleation of a Volterra dislocation dipole. (c) η calculated using linear stability of FDM, for velocity field in (a). (d) η, for velocity field in (b); The yellow-lines in (b) and (d) show the position of the slip embryo. Because of the continuously distributed slip distribution as shown in case (a) η is non-local as shown in (c). On the other hand, in (d) η is localized at the points of nucleation because of sharp drop-offs in slip at the boundary of embryo in (b).

field with respect to some planes. Here, by a phase boundary we mean a single surface in the body across which the deformation gradient is discontinuous; by a shear band we mean two such surfaces separated by a small distance, and 'non-terminating' refers to the fact that these discontinuity surfaces run from one external surface of the body to another. Maloney et al. [14] defined Ω as the transverse derivative of the velocity field with respect to the slip direction to identify location of dislocation nucleation. The Ω field in Fig. 8b is high for the long-wavelength mode shown in Fig. 8a, that is not a case of nucleation of dislocation dipole. Fig. 8a shows a smooth buckling mode from a state of homogeneous compression. The mode is the linearized

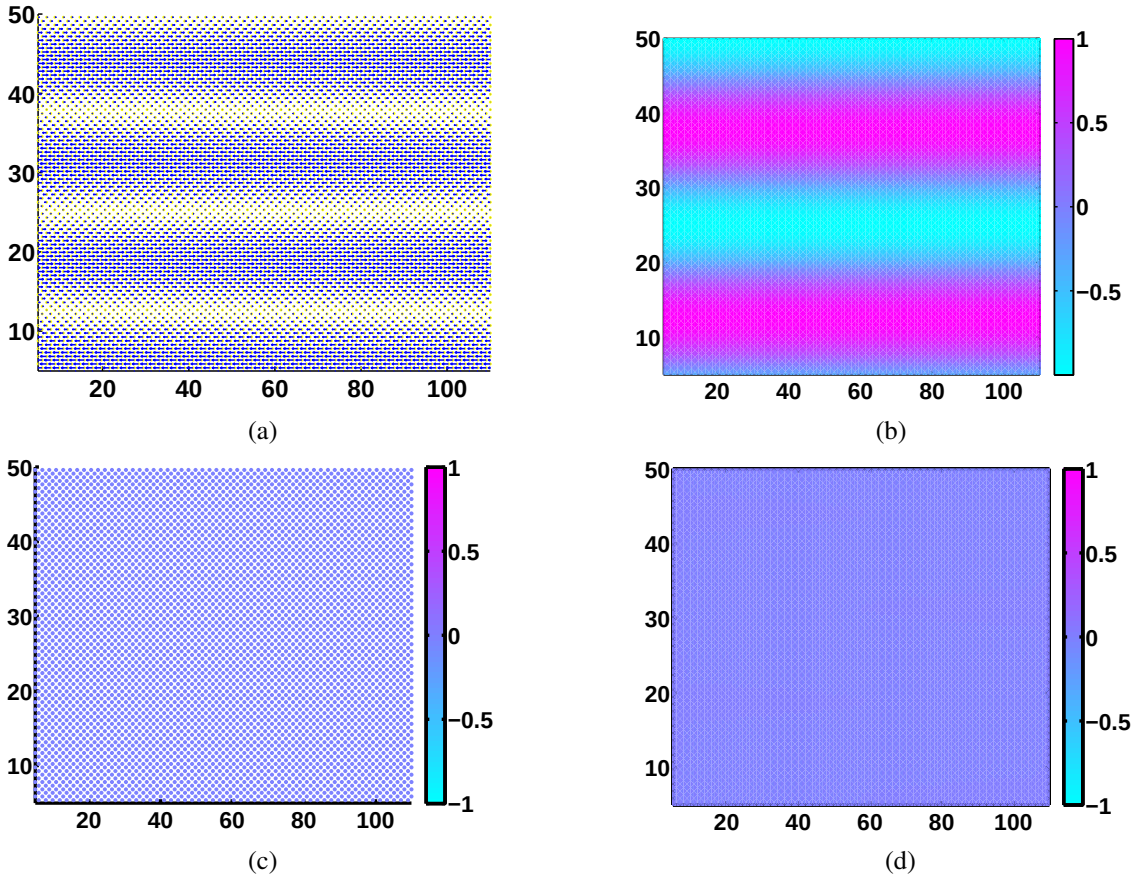

Fig. 8: L-J crystal, O_2 (a) Critical eigenmode for homogeneous compression just before bifurcation. (b) Ω/Ω_{max} corresponding to the mode. (c) Λ, Λ decreases by an order of magnitude and is almost zero in the whole configuration just before bifurcation. (d) η, η is almost zero everywhere and does not show dislocation nucleation.

precursor of a long-wavelength nonlinear instability that occurs in this simulation with a flat indenter. Note that in the case of homogeneous compression the critical mode is completely non-local and extends to full system size, as compared to the critical mode for nano-indentation discussed in Sec. II-A. In this case of the long-wavelength instability, η is close to 0 and does not predict dislocation nucleation as shown in Fig. 8d. In the case of a simple shear where $v_{1,2}$ is non-zero and $v_{1,1}$ is zero, η would be zero, whereas Ω would be high.

For this case of homogeneous compression, Λ is almost 0 in the entire configuration as shown in Fig. 8c. Since Λ is 0, it is reasonable to check whether a localized velocity mode with polarization and plane normal predicted using Λ is also an eigenmode of the discrete atomistic Hessian matrix, as a check of the adequacy of local continuum elastic response in reflecting

the elasticity and instabilities of the atomic lattice. As alluded to in the previous paragraph, we verified that a localized shear band mode predicted by the continuum analysis is *not* an eigenmode of the atomistic stiffness matrix even though Λ is 0. This difference can be attributed to the atomistic details in the stiffness or the Hessian matrix; roughly speaking, an atomistic model may be assumed to correspond to higher than second-order boundary value problems and the linearization of such a system governing instabilities is naturally different from that of the corresponding second-order system. This analysis suggests that Λ cannot always be used even for the case of phase boundary nucleation. Moreover, in this case of homogeneous compression, Λ is critical i.e. 0 everywhere and its critical eigenmode does not correspond to the nucleation of a dislocation dipole.

E. Hydrostatic Compression

In the fully 3-D simulations if a pure hydrostatic velocity field is considered, then

$$v_{j,m} = e\delta_{jm} \tag{32}$$

where, e is a constant and (26) becomes

$$\frac{da_{ij}}{dt} = -2ea_{ij}. \tag{33}$$

Since e is negative for compression, a_{ij} always shows growth. As shown in sec. V, our analysis requires η should grow by orders of magnitude for implying dislocation nucleation. In this case of hydrostatic compression, if the compression rate is uniform then η would be constant and would not indicate nucleation. However, by the same token, were a non-uniform-in-time, purely hydrostatic compression state to be achieved in a real deformation, then the FDM based indicator would imply growth of dislocation density.

Leaving aside the question of the physical merit of this case, the reason behind this awkward implication may be understood as follows. From a dislocation-free state, a governing constraint behind the prediction of growth of dislocation perturbations is (28) which is equivalent to

$$\frac{d}{dt}\int_{p(t)} \alpha n \, da = 0$$

for any material area patch $p(t)$ in the body, and the net Burgers vector of any area patch is conserved. Thus, if a deformation tends to shrink areas then the dislocation density has to grow to conserve the Burgers vector content of the perturbation. Interestingly, it appears that it is this kinematic 'mechanism' that predicts correct trends for the initiation of dislocation nucleation as shown in the results of this paper. Of course, once the dislocation density perturbation grows, subsequent states of evolution have non-zero dislocation density and then Burgers vector content of area patches is also affected by the flow term $\alpha \times V$ and its spatial variation.

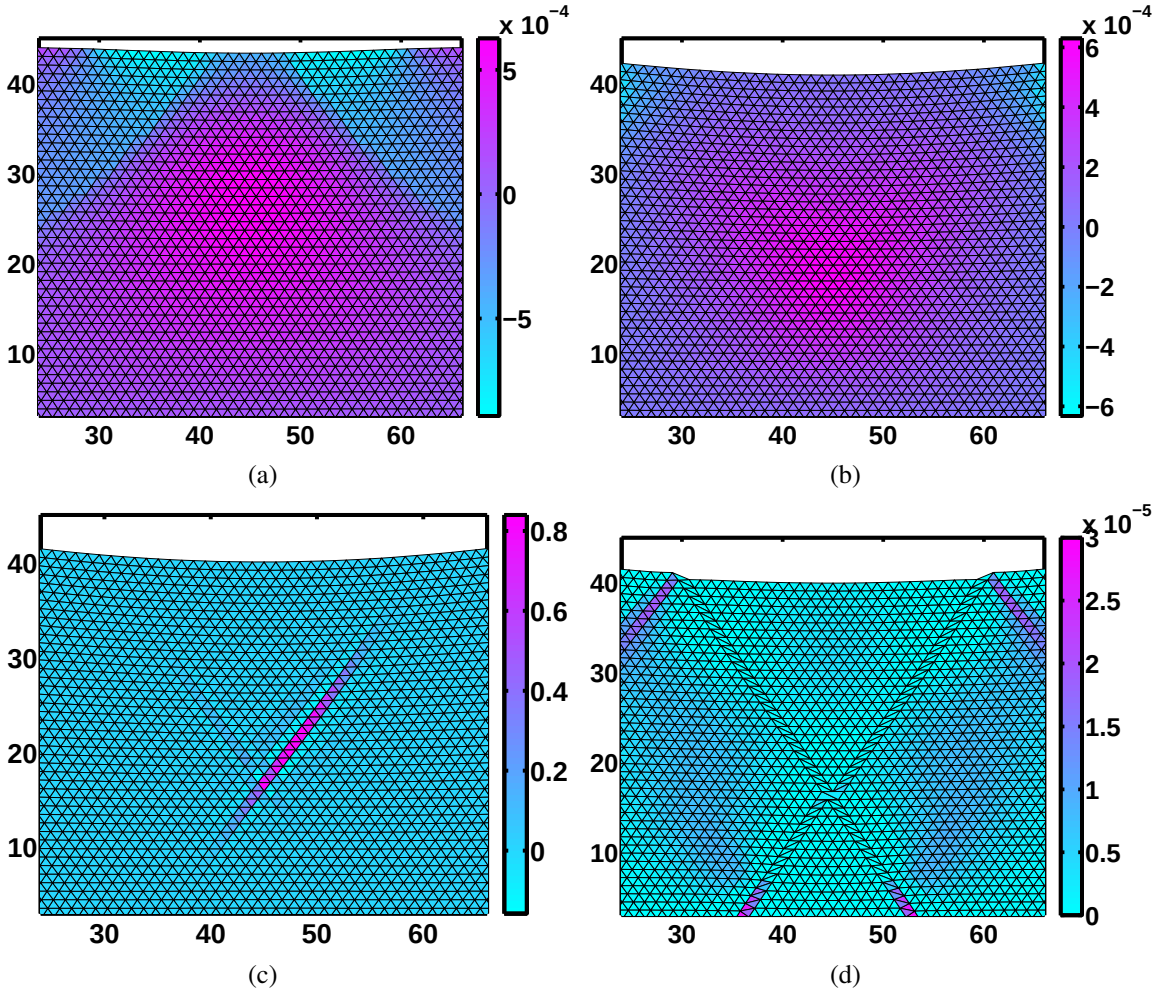

Fig. 9: η calculated using linear stability of FDM for L-J crystal, O_1, $R = 120$ in (a),(b) much before dislocation nucleation event; (c) just before nucleation; (d) after nucleation. η is precisely maximum at the embryo. It decreases by order of magnitudes after nucleation.

V. Results

We mesh both two and three dimensional systems using Delaunay triangulation. Using sec. II-A, particle velocities are known at each atom or node. We use linear shape functions to interpolate these velocities on each element and compute derivatives. The velocity derivatives are needed to calculate the maximum positive real part of eigenvalues of $\mathscr{N}$, η, at the centroid of each triangle (in 2D) or tetrahedron (in 3D). In all figures in this work, the arrows correspond to the particle velocity. In two dimensional simulations, there are two planes of atoms slipping against each other as shown in Fig. 4 and give rise to a pair of dislocations.

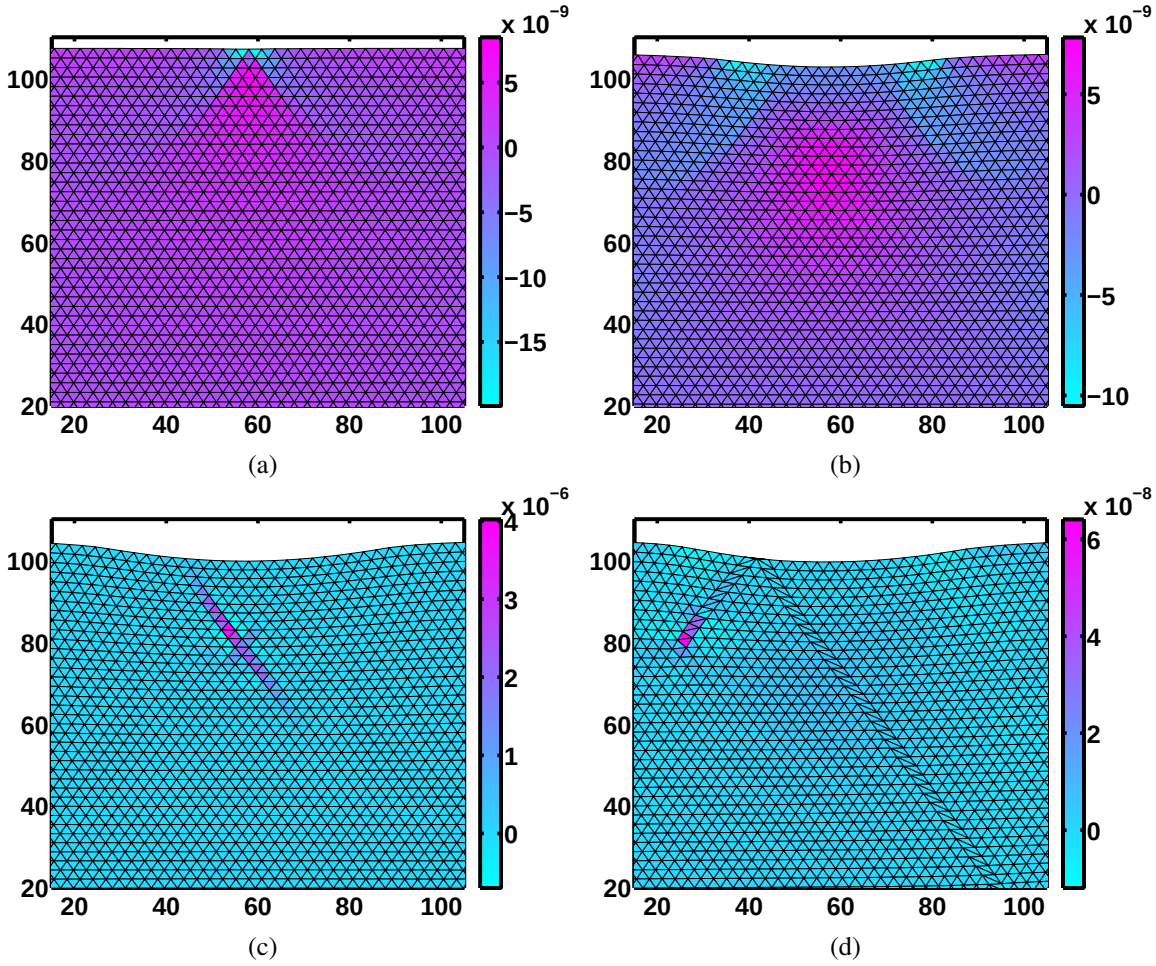

Fig. 10: η calculated using linear stability of FDM for EAM-Al. crystal, O_1, $R = 40$ in (a),(b) much before dislocation nucleation event; (c) just before nucleation; (d) after nucleation. η is precisely maximum at the embryo. It decreases by order of magnitudes after nucleation.

For orientation O_1, the spatial η field is shown at various indenter depths for L-J crystal in Fig. 9. η is around 6×10^{-4} much before nucleation as shown in Figs. 9a and 9b. Note that positive η does not necessarily imply nucleation, this being a limitation of constant-coefficient linear stability analysis. Just before nucleation, η increases by three orders of magnitude. Also, it is highly positive only for the triangles formed by atoms on the slipping planes. After nucleation, η decreases by four orders of magnitude and does not persist at the dislocation cores. In Fig. 10, we show similar analysis for EAM-Al crystals. Initially η is around 6×10^{-9} and just before nucleation it increases by three orders of magnitude. Similar to L-J, for the EAM-Al crystal, η drops by three orders of magnitude after nucleation. Similar results are observed for L-J

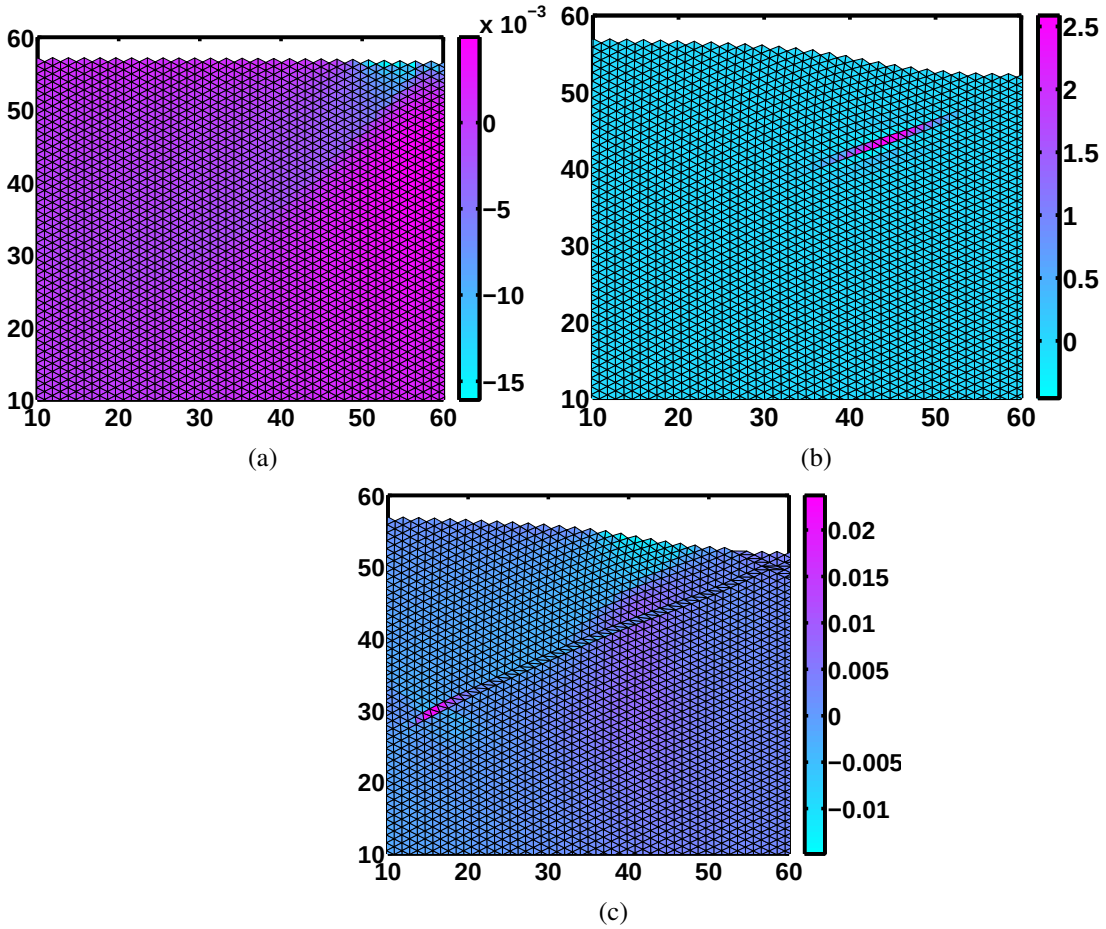

(a) (b)

(c)

Fig. 11: η calculated using linear stability of FDM, for L-J crystal, O_2, $R = 50$ in (a) much before dislocation nucleation event; (b) just before nucleation; (c) after nucleation. η is precisely maximum at the embryo. It decreases by order of magnitudes after nucleation. Only one-half of the crystal in which dislocation nucleation happens is shown.

O_2 orientation in Fig. 11. Even though before nucleation η depends on the crystal orientation and inter-atomic potential, it increases by three orders of magnitude just before nucleation and decreases by the same amount after nucleation for all systems in 2D.

In Fig. 12a, 12b and 12d, results for the fully 3D simulations are shown. In these figures the FCC lattice is sliced along the plane containing the unstable embryo. In Fig. 12a the colors represent the magnitude of velocity field. Long before nucleation, η is around 3×10^{-7}. Just before nucleation, η increases by two order of magnitude as shown in Fig. 12b and then, after nucleation it drops by roughly two orders of magnitude as in Fig. 12d.

For predicting the line direction, l, we calculated the eigenmodes of $\mathscr{N}$. The eigenmodes

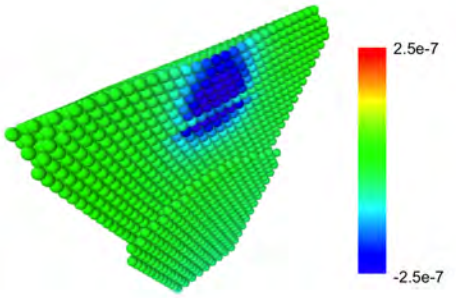

(a)

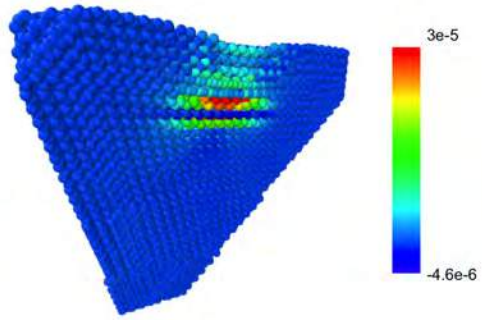

(b)

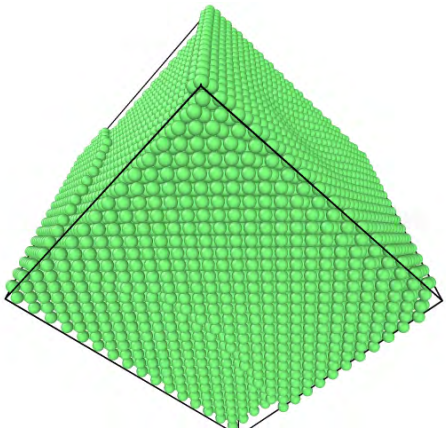

(c)

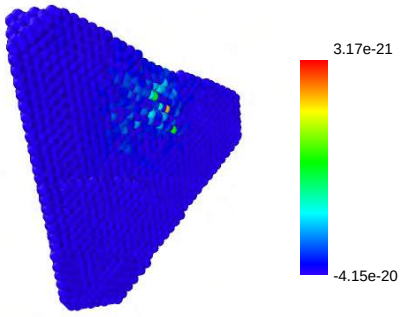

(d)

Fig. 12: L-J 3D - FCC crystal, $R = 25$. Indentation axis is along [1 0 0] axis. The crystal is sliced along the plane (111). The colors represent: (a) Velocity field magnitude; (b) η, note that the balls plotted in this figure are located at the centroid of tetrahedrons formed by atoms where η is calculated. Similar to 2D, in fully 3D simulations η increases by two orders of magnitude just before nucleation and it decreases by two orders of magnitude after nucleation. The full FCC Lattice is shown in (c). There are periodic boundaries conditions in the normal directions to the indentation axis. Black solid lines in (c) show the periodic box size. (d) η computed by substituting the Convected rate by Jaumann rates in the linear stability analysis of FDM. Interestingly only the emergent convected rates from linear stability analysis show instability.

correpond to the nucleating dislocation density tensor. At the points of interest, $\mathscr{N}$ had more than one eigenvalues with positive real part. We verified that the nucleating dislocation density tensor lies in the linear span of the eigenmodes of the eigenvalues with positive real parts. An expression for predicting the line direction, l, was formulated in [19] as shown in (34). This expression is related to the stress gradient criterion described in Sec. III and is given by

$$l = grad\tau \times n. \tag{34}$$

τ is the resolved shear stress on the slip plane with normal n. We find that (34) predicts the line direction correctly only for edge dislocations, where the line direction is normal to the Burgers vector. For mixed dislocations, the stress gradient criterion predicts only the edge component of the actual line direction.

In (25) the convected rate emerges naturally. If we replace the convected rate by the analog of the Jaumann rate for a two-point tensor, $\mathscr{N}$ becomes a skew-symmetric matrix. A skew-symmetric matrix always has imaginary eigenvalues and can never be positive-definite. Hence, the Jaumann rate based $\mathscr{N}$ cannot predict nucleation. The numerical result for maximum eigenvalue of the Jaumann rate based $\mathscr{N}$, just before nucleation, is also shown in Fig. 12d. As the discussion surrounding (30) shows, it does not predict nucleation.

VI. Concluding Remarks

The kinematics of dislocation density evolution in FDM appears to be sufficiently versatile in embodying homogeneous dislocation nucleation within the theory and for developing criteria that can be used in other modeling paradigms. In order to isolate and understand this capability, we have tested the feature with atomistically generated velocity fields that, obviously, have analogs in coarser-than-atomic-scale simulation models like Discrete Dislocation Dynamics and Field Dislocation Mechanics. In this sense, our analysis represents an advance in putting forward a conceptual framework for dislocation nucleation that naturally connects to coarser scale models. A main question that arises at this point is the extent to which these coarser length scale models can produce the requisite material velocity fields. Clearly, nonlinear kinematics is important and our analysis in Sec. IV-D shows that dislocation nucleation criteria and associated velocity modes based on classical ideas of loss of strong ellipticity of nonlinear elastic models, even when driven by atomistic input through the Cauchy-Born (CB) hypothesis, may not always be adequate. However, during nano-indentation simulations that induce a strong inhomogeneous deformation, sufficiently close to the bifurcation point of the lattice statics calculation, the polarization direction and discontinuity-plane normal predicted from the (continuum) acoustic tensor corresponding to Λ predicts the correct slip plane and Burgers vector direction for the nucleating dislocation dipole. This holds irrespective of the crystallographic orientation and inter-atomic potential. Based on this evidence, dislocation nucleation criteria relying on velocity fields generated from CB-based continuum elasticity *coupled* with the FDM-based dislocation nucleation indicator we have developed herein appears to be a logical step to pursue in future work. Furthermore, higher-order elasticity can be folded into a framework like Field Dislocation Mechanics and even without resorting to nonlocal/gradient elasticity, FDM in the

finite deformation setting incorporating a dislocation density contributing to core energy has a significantly different stress response function [18] than the classical case. The effect of such enhancements in predicted velocity fields from full nonlinear analyses remain to be explored.

VII. Acknowledgments

This material is based upon work supported by the National Science Foundation under Award Number CMMI-1100245.

References

[1] W. W. Gerberich, J. C. Nelson, E. T. Lilleodden, P. Anderson, and J. T. Wyrobek, "Indentation induced dislocation nucleation: The initial yield point," *Acta Materiala*, vol. 44, p. 35853598, Sept. 1996.

[2] C. A. Schuh, J. K. Mason, and A. C. Lund, "Quantitative insight into dislocation nucleation from high-temperature nanoindentation experiments," *Nature Materials*, vol. 4, p. 617621, Aug. 2005.

[3] O. Rodriguez de la Fuente, J. A. Zimmerman, M. A. Gonzalez, J. de la Figuera, J. C. Hamilton, W. W. Pai, and J. M. Rojo, "Dislocation emission around nanoindentations on a (001) fcc metal surface studied by scanning tunneling microscopy and atomistic simulations," *Physical Review Letters*, vol. 88, p. 036101, Jan. 2002.

[4] K. Van Vliet, J. Li, T. Zhu, S. Yip, and S. Suresh, "Quantifying the early stages of plasticity through nanoscale experiments and simulations," *Physical Review B*, vol. 67, Mar. 2003.

[5] R. E. Miller and A. Acharya, "A stress-gradient based criterion for dislocation nucleation in crystals," *Journal of the Mechanics and Physics of Solids*, vol. 52, p. 15071525, 2004.

[6] J. Li, K. J. Van Vliet, T. Zhu, S. Yip, and S. Suresh, "Atomistic mechanisms governing elastic limit and incipient plasticity in crystals," *Nature*, vol. 418, pp. 307–310, July 2002.

[7] R. Miller and D. Rodney, "On the nonlocal nature of dislocation nucleation during nanoindentation," *Journal of the Mechanics and Physics of Solids*, vol. 56, pp. 1203–1223, Apr. 2008.

[8] J. R. Rice and G. E. Beltz, "The activation energy for dislocation nucleation at a crack," *Journal of the Mechanics and Physics of Solids*, vol. 42, pp. 333–360, Feb. 1994.

[9] J. R. Rice, "Dislocation nucleation from a crack tip: An analysis based on the peierls concept," *Journal of the Mechanics and Physics of Solids*, vol. 40, pp. 239–271, Jan. 1992.

[10] R. Peierls, "The size of a dislocation," *Proceedings of the Physical Society*, vol. 52, no. 34, 1940.

[11] F. R. N. Nabarro, "Dislocations in a simple cubic lattice," *Proceedings of the Physical Society of London*, vol. 59, no. 332, p. 256272, 1947.

[12] V. Vitek, "Intrinsic stacking faults in body-centered cubic crystal," *Philosphical Magazine*, vol. 18, no. 154, p. 773&, 1968.

[13] R. Hill, "Acceleration waves in solids," *Journal of the Mechanics and Physics of Solids*, vol. 10, pp. 1–16, Jan. 1962.

[14] A. Garg, A. Hasan, and C. Maloney, "Universal scaling laws for homogeneous disocation nucleation during nano-indentation," in preparation.

[15] A. Acharya, "A model of crystal plasticity based on the theory of continuously distributed dislocations," *Journal of the Mechanics and Physics of Solids*, vol. 49, no. 4, p. 761784, 2001.

[16] A. Acharya, "Constitutive analysis of finite deformation field dislocation mechanics," *Journal of the Mechanics and Physics of Solids*, vol. 52, no. 2, p. 301316, 2004.

[17] A. Acharya, "Jump condition for GND evolution as a constraint on slip transmission at grain boundaries," *Philosphical Magazine*, vol. 87, no. 8-9, p. 13491359, 2007.

[18] A. Acharya, "Microcanonical entropy and mesoscale dislocation mechanics and plasticity," *Journal of Elasticity*, vol. 104, no. 1-2, pp. 23–44, 2011.

[19] A. Acharya, A. Beaudoin, and R. Miller, "New perspectives in plasticity theory: Dislocation nucleation, waves, and partial continuity of plastic strain rate," *Mathematics and Mechanics of Solids*, vol. 13, no. 3-4, p. 292315, 2008.

[20] S. Plimpton, "Fast parallel algorithms for short-range molecular dynamics," *Journal of Computational Physics*, vol. 117, pp. 1–19, Mar. 1995.
[21] F. Ercolessi and J. B. Adams, "Interatomic potentials from first-principles calculations," *MRS Online Proceedings Library*, vol. 291, pp. null–null, 1992.
[22] A. Lemaitre and C. Maloney, "Sum rules for the quasi-static and visco-elastic response of disordered solids at zero temperature," *Journal of Statistical Physics*, vol. 123, pp. 415–453, Apr. 2006.
[23] J. R. Willis, "Hertzian contact of anisotropic bodies," *Journal of the Mechanics and Physics of Solids*, vol. 14, pp. 163–176, May 1966.
[24] R. Phillips, *Crystals, Defects and Microstructures: Modeling Across Scales*. Cambridge: Cambridge University Press, 2001.
[25] J. Li, T. Zhu, S. Yip, K. J. Van Vliet, and S. Suresh, "Elastic criterion for dislocation nucleation," *Materials Science and Engineering: A*, vol. 365, pp. 25–30, Jan. 2004.
[26] J. Zimmerman, C. Kelchner, P. Klein, J. Hamilton, and S. Foiles, "Surface step effects on nanoindentation," *Physical Review Letters*, vol. 87, Oct. 2001.
[27] R. Hill, "Aspects of invariance in solid mechanics," *Advances in applied mechanics*, vol. 18, pp. 1–75, 1978.